33RD CONGRESS
OF THE INTERNATIONAL COUNCIL
OF THE AERONAUTICAL SCIENCES
STOCKHOLM, SWEDEN, 4-9 SEPTEMBER, 2022

ICAS 2022 SWEDEN

A REDUCED ORDER MODEL FOR FULL-SCALE DRONE COLLISIONS

Florian Franke[1,2], Uli Burger[2], Christian Hühne[1,3]

[1]TU Braunschweig, Universitätsplatz 2, 38106 Braunschweig, Germany
[2]TH Ingolstadt, Esplanade 10, 85049 Ingolstadt, Germany
[3]DLR, Lilienthalplatz 7, 38108 Braunschweig, Germany

Abstract

Drones are an increasing threat for manned aviation. A collision with a drone may lead to catastrophic or even fatal accidents. Current analyses of drone collisions are based on tests and simulations. Such investigations are time and cost expensive. These methods are not suitable for a rapid load estimation in the framework of a preliminary design. Due to this, a simple analytic reduced order model for drone collisions is developed. This drone strike model is a superposition of two existing impact models. It can be used to determine the impact force between the drone projectile and a target structure. The drone strike model depends on the target behavior. If the target is sufficiently rigid, the impact is defined as soft. Otherwise it is a hard impact. The calculation results are compared with results from finite element impact simulations of a full drone with three different targets: a rigid wall, a generic flat aluminum plate and a generic wing leading edge. The impact velocities and flight orientations of the drone are varied. The results show a good agreement between the drone strike model results and simulations in case of a soft impact and high velocities. A damage model of the target is not included into the drone strike model what leads to larger deviations in case of hard impacts. It can be concluded that the drone strike model is suitable to study the influence of design changes on the impact force with a minimum calculation effort.

Keywords: Drone collision, Unmanned aerial vehicle, Analytic approach, Impact force, FEM

1 Introduction

Small unmanned aerial vehicles (sUAV), or so-called drones, are an increasing threat for manned aviation. Drone incidents increase, as UK Airprox Board and German Air Traffic Control data show [1; 2]. Drones are often piloted by hobby pilots who do not know the applicable regulations and fly their drone in dangerous areas. In parallel to bird strikes and hailstorms, a drone may impact an aircraft, which can lead to catastrophic or even fatal accidents. The differences between drone strikes and well-known bird strikes are that current aircraft structures are designed to withstand bird strikes, not drone strikes. Furthermore, a bird consists out of 90 Vol% water, whereas multiple solid components form the drone. The effects of such collisions can be investigated with laboratory tests and numerical simulations. Both of them are expensive, regarding time and costs. Due to this fact, a new analytic model of reduced order was developed to investigate drone collisions and determine the impact force between target and drone projectile. The objective of this paper is to apply this so-called “Drone Strike Model” (DSM) on full-scale drone collisions. This paper builds on results from [3–5].

In this work, we use the terms drone strike and drone collision. Both describe the impact of an sUAV with a manned aircraft. A small UAV is a drone with a maximum take-off weight of 1.5 kg, as it is defined by [6]. The vast majority of studies on drone strikes have been done with tests or finite element (FE) simulations. Gettinger et al. [7] was the first author who studied drone strikes with FE simulations.

Song et al. [8–11], Lyons et al. [12], Liu and Man et al. [13–17], Hou et al. [18] as well as Yu et al. [19] studied drone strikes with aircraft engines. Furthermore, Wang et al. [20], Drumond et al. [21–23], Meng et al. [24], Lu et al. [25; 26], Dadouche et al. [27] and Harker et al. [28] focused their work on impacts with aircraft structures. Other authors like Ritt, Jonkheijm and Slowik analyzed impacts on helicopter structures [29–32]. A lot of relevant work regarding impact tests and simulations has been done by ASSURE (Alliance for System Safety of UAS through Research Excellence). They published four reports about their drone strike research results [6; 33–35]. From the studies reviewed here, it is evident that none of the authors studied drone strikes with an analytic model. An analytic model has cost and time advantages compared to tests and simulations and is therefore particularly suitable for use in preliminary design.

Within this paper, we use the drone strike model, which is discussed in chapter 2. The drone strike model will be compared with finite element simulation results from impacts with various structures. Chapter 3 shows the FE models. In chapter 4, the results from both the DSM and the FEA (finite element analysis) are compared.

2 The Drone Strike Model

A drone collision represents a multi-body impact. The components of the drone hit the target one after the other. In general, the DSM is a superposition of two existing models. A drone consists out of several components. These components have different impact behaviors. For example, a motor is made out of cast aluminum and a solid steel core. It will show plastic deformations but the structure still exists after the impact process. On the other hand, the shell and the battery will show a fragmenting behavior. That means, that these components will shatter and only small fragments are present after the impact. Each component impact behavior is modeled with a specific model. If the component shows a non-fragmenting behavior, a spring-mass impact model is used. If the component shatters, the so-called “Aircraft Impact Model” (AIM) is used. Furthermore, the DSM depends on the target behavior. If the target structure is sufficiently rigid, then the impact can be defined as soft. Otherwise, the impact is defined as a hard impact. Both are described in the following chapters.

2.1 Drone Strike Model for Rigid Targets

In case of a rigid and stationary target, only the projectile determines the impact force. The drone projectile is simplified to a 1-D line model. A mass- and a burst load distribution are determined along this line. The drone is divided into two areas along the line, dependent from the impact behavior of the single components. The shell will shatter during the impact and can therefore be modeled with the AIM, as it can be seen in Figure 1 (Area 1). Motors are attached to the shell. They show mainly plastic deformations. Their impacts can be modeled with a spring-mass model. Within area 2, both models are superimposed. This leads to the following equations for the DSM in case of a rigid target:

$$P(t) = \begin{cases} P_\mathrm{c}\big(x(t)\big) + \mu\big(x(t)\big) \cdot v(t)^2 & \text{for} \quad x < x_{\mathrm{ma},i} \ \vee \ x_{\mathrm{me},i} < x < x_{\mathrm{ma},i+1} \ \vee \ x_{\mathrm{me},i+n} < x \\ P_\mathrm{c}\big(x(t)\big) + \mu\big(x(t)\big) \cdot v(t)^2 + P_\mathrm{S}\big(v(t), x(t)\big) & \text{for} \quad x_{\mathrm{ma},i} \le x \le x_{\mathrm{me},i} \end{cases} \tag{1}$$

$$P_\mathrm{S} = v_\mathrm{i} \sqrt{k_\mathrm{e} \cdot m_\mathrm{pnf}} \cdot \sin\left(\frac{\pi}{t_\mathrm{f}} \cdot (t - t_0)\right) \tag{2}$$

In these equations P represents the contact force; P_c is the burst load distribution; μ is the mass distribution; v is the velocity of the undamaged part of the projectile; P_S is the force from the spring-mass model. The spring-mass model uses the current velocity of projectile as the initial impact velocity v_i; k_e is the substitute stiffness of the spring; m_pnf is the mass of the non-fragmenting projectile; t_f describes the impact duration and t_0 is a reference time.

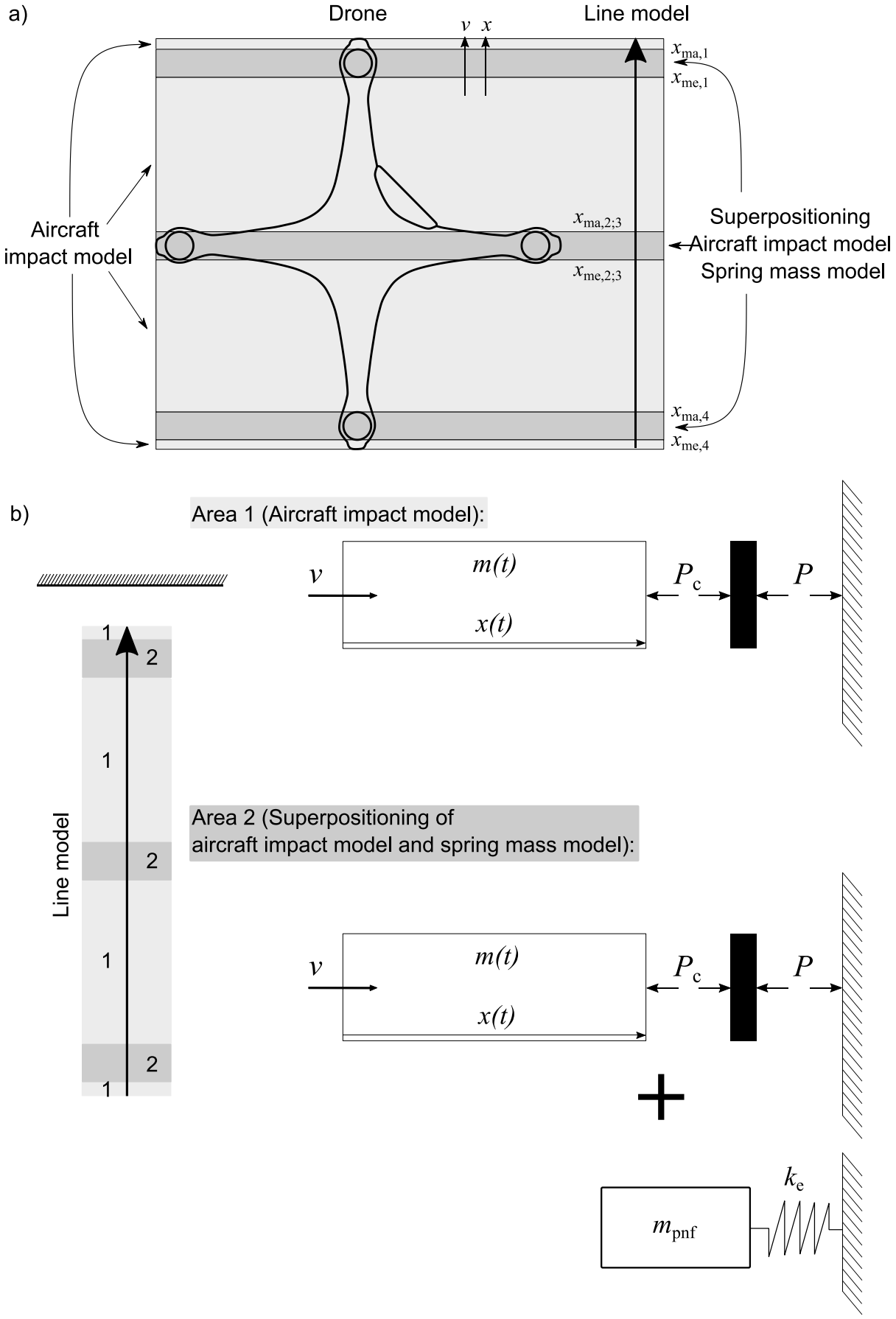

Figure 1: Mechanical substitute model for soft impacts

2.2 Drone Strike Model for Deformable Targets

In case of a hard impact, the model must be modified and the target behavior must be incorporated. A spring-mass-damper system is suitable to model the target behavior. The DSM of the rigid plate is therefore extended by a spring-mass model of the target structure. In this model, m_t is the target mass, k_t is the target spring stiffness and c_t is the damping of the target. The projectile is described as a 1-D line model. The following equations (3) and (4) are the DSM in case of a soft impact. Figure 2 illustrates the mechanical substitute model for hard impacts.

$$P(t) = \begin{cases} P_\mathrm{c}\big(x(t)\big) + \mu\big(x(t)\big) \cdot v(t)^2 & \text{for} \quad x < x_{\mathrm{ma},i} \ \vee \ x_{\mathrm{me},i} < x < x_{\mathrm{ma},i+1} \ \vee \ x_{\mathrm{me},i+n} < x \\ P_\mathrm{c}\big(x(t)\big) + \mu\big(x(t)\big) \cdot v(t)^2 + P_\mathrm{S}\left(\dfrac{\mathrm{d}x}{\mathrm{d}t}, x(t)\right) & \text{for} \quad x_{\mathrm{ma},i} \le x \le x_{\mathrm{me},i} \end{cases} \tag{3}$$

$$P_\mathrm{S} = \left(\frac{\mathrm{d}x}{\mathrm{d}t}(t_0)\right)\sqrt{k_\mathrm{e} \cdot m_\mathrm{pnf}} \cdot \sin\left(\frac{\pi}{t_\mathrm{f}} \cdot (t - t_0)\right) \tag{4}$$

The relative velocity $\mathrm{d}x/\mathrm{d}t$ can be determined with the following two differential equations ([36]):

$$\frac{\mathrm{d}^2x}{\mathrm{d}t^2} = \frac{P_\mathrm{c}\big(x(t)\big)}{m(t)} + \frac{P_\mathrm{c}\big(x(t)\big)}{m_\mathrm{t}} + \frac{\mu\big(x(t)\big)}{m_\mathrm{t}}\left(\frac{\mathrm{d}x}{\mathrm{d}t}\right)^2 - \frac{c_\mathrm{t}}{m_\mathrm{t}} \cdot \frac{\mathrm{d}y}{\mathrm{d}t} - \frac{k_\mathrm{t}}{m_\mathrm{t}} y(t) \tag{5}$$

$$\frac{\mathrm{d}^2y}{\mathrm{d}t^2} = \frac{P_\mathrm{c}\big(x(t)\big)}{m_\mathrm{t}} + \frac{\mu\big(x(t)\big)}{m_\mathrm{t}}\left(\frac{\mathrm{d}x}{\mathrm{d}t}\right)^2 - \frac{c_\mathrm{t}}{m_\mathrm{t}} \cdot \frac{\mathrm{d}y}{\mathrm{d}t} - \frac{k_\mathrm{t}}{m_\mathrm{t}} y(t) \tag{6}$$

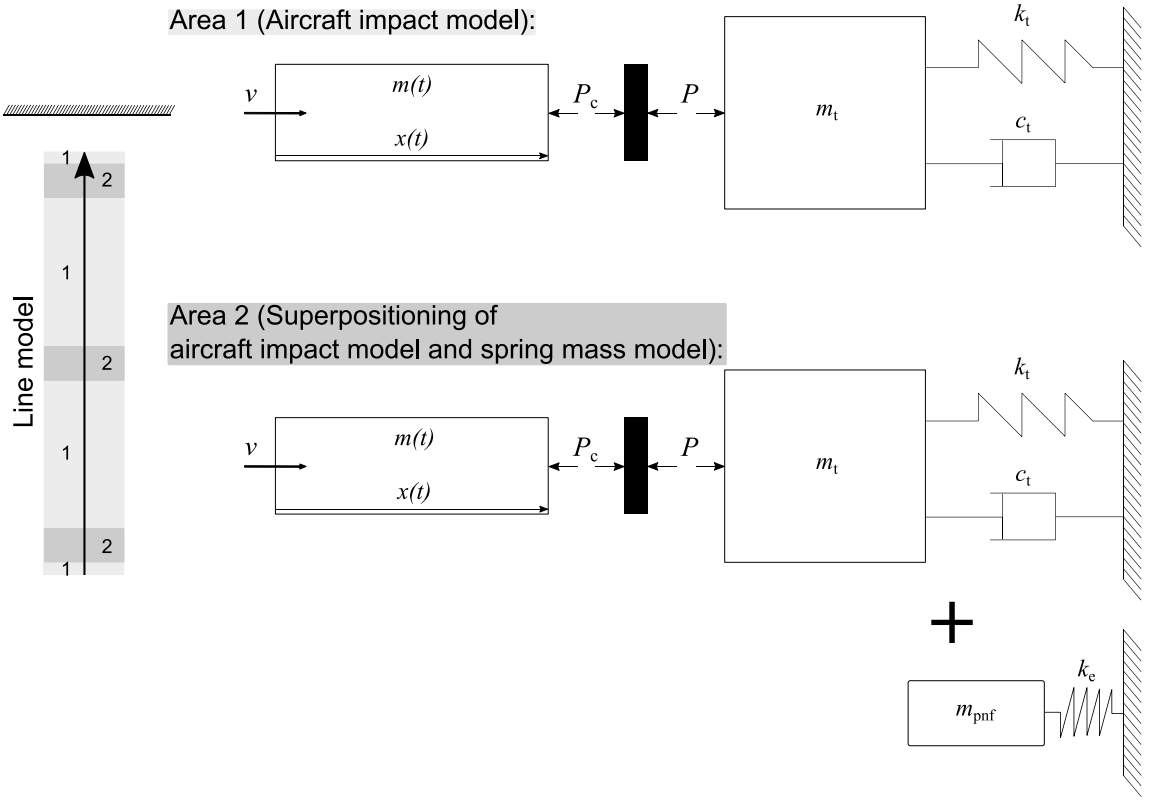

Figure 2: Mechanical substitute model for hard impacts

2.3 Drone Strike Model Input Parameters

As described above, the model needs certain input parameters. A mass as well as a burst load distribution of the components with a fragmenting damage behavior are needed. The mass distribution can be determined with the FE preprocessor. The burst load is determined analytically with the material yield stress multiplied with a reduction factor due to geometry nonlinearities. This reduction factor was determined to be 0.25 in this case. Both distributions are shown Figure 3. They depend on the flight orientation α of the drone.

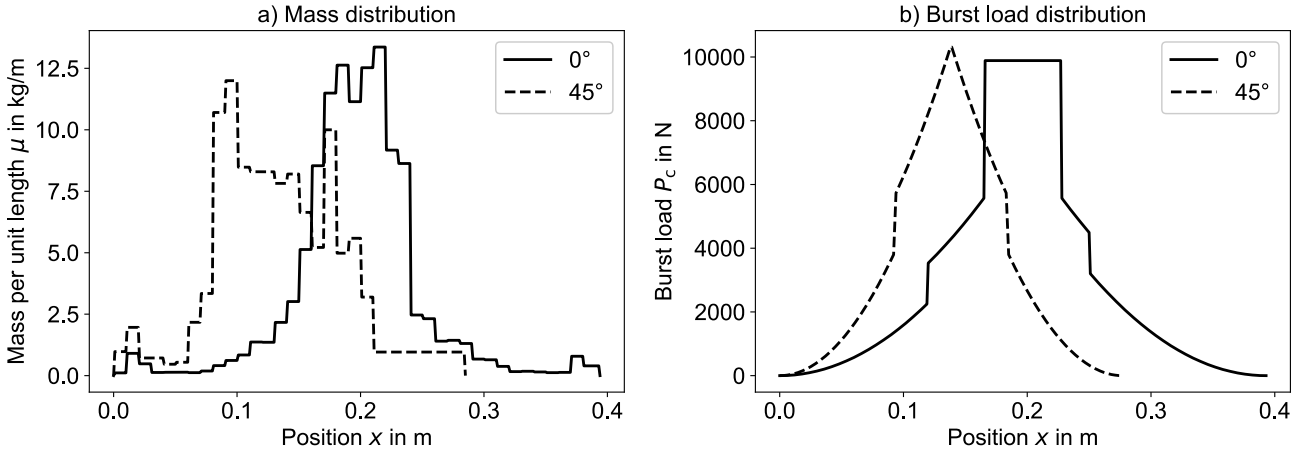

Figure 3: Mass- and burst load distribution

The full drone has a mass of 1.38 kg. Each motor has a mass of 0.043 kg. The generic Al2024-T3 target has a mass of 1.76 kg and the wing leading edge model weighs 17.43 kg. Preliminary tests show, that the impact of a motor with the rigid wall lasts 0.107 ms. In case of an Al2024-T3 target structure, it takes 0.326 ms. The substitute stiffness is 12701.2 kN/m for a soft impact and 1111.2 kN/m for a hard impact. We use the Runge-Kutta-45 method to calculate the DSM results. The termination conditions are either $x(t) = 0$ or $\mathrm{d}x/\mathrm{d}t = 0$.

3 Finite-Element-Models

3.1 FE-Models of Projectiles and Components

In this work, we follow a stepwise approach to investigate drone strikes with finite element models. First of all, the impact of a full-scale drone with rigid targets is analyzed. A DJI Phantom 4 drone model is studied. Finite element simulation data are compared with results from the analytic drone strike model for soft impacts. On a second step, we investigate the impact of the drone with a generic aluminum Al2024-T3 plate. This material is being investigated as it is a typical aeronautical material. Finally, the impact on a generic wing leading edge (WLE) is studied. Four impact speeds and two flight orientations of the drone are simulated on every level. The impact speeds are 20, 80, 100 and 150 m/s. We investigate the relative velocity. The targets are stationary, only the projectile moves. The investigated flight orientations of the drone are 0° and 45°. The lowest velocity may be compared to a helicopter in hover flight. Typical aeronautical materials show perforation damage at the highest investigated impact velocity. The following Figure 4 shows the stepwise approach.

A simplified model of the DJI Phantom 4 is used for the investigations. Five different components form this model: The top- and bottom shell, the motors, the battery and the landing gear (Figure 5). The numerical models of the drone components are validated with quasi-static data. Other components, such as the camera, rotors or electrics, are neglected. The masses of the neglected components are evenly distributed around the center of gravity of the drone model by increasing the density of the shell. Fully integrated solid and shell elements are used to avoid hourglassing.

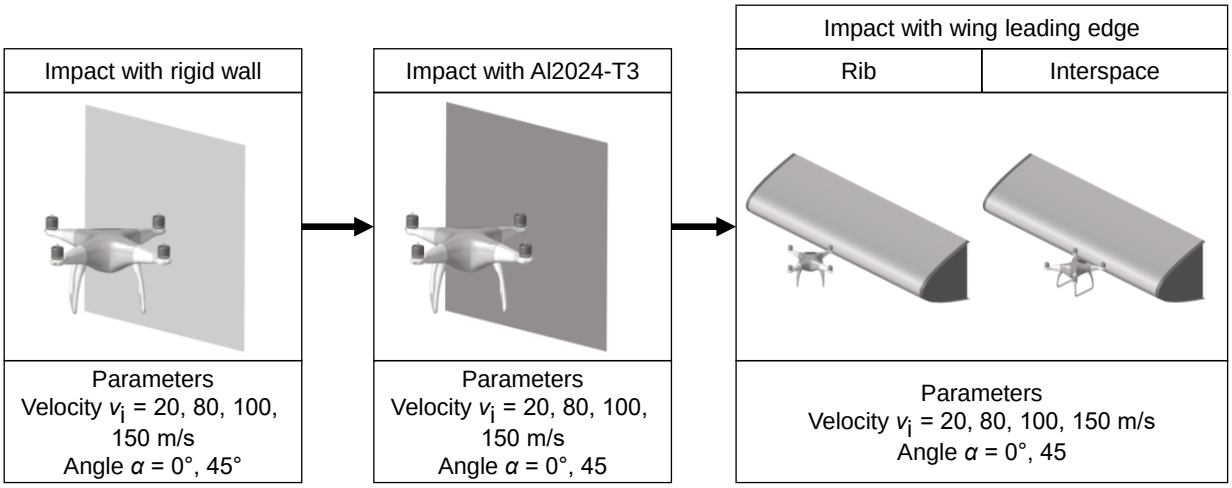

Figure 4: Stepwise approach to calculate the full-scale drone impact

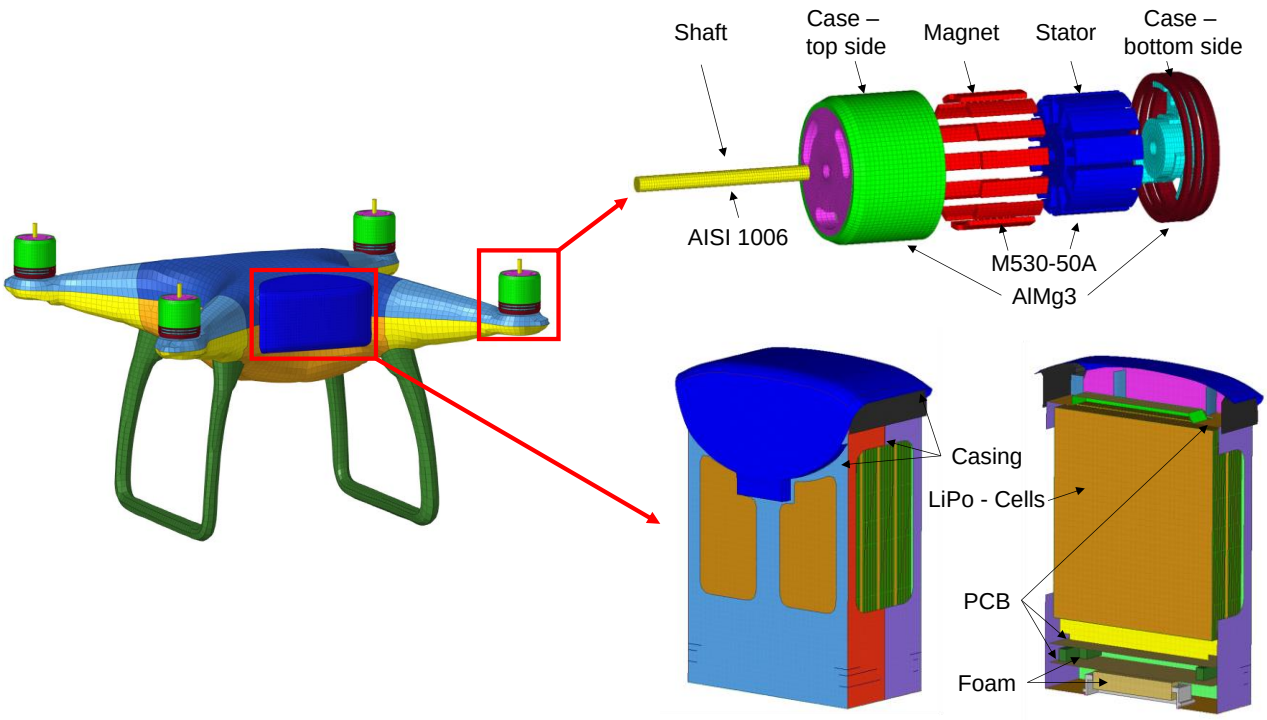

Figure 5: Finite-Element-Model of the DJI P4 [4]

The rigid wall as well as the aluminum target are simple rectangular plates (500 mm x 500 mm). The aluminum plate has a thickness of 2.54 mm. The edges are clamped. The WLE is a generic model. It has a width and a height of 400 mm and a length of 1500 mm (Figure 6). It consists out of skin, ribs and spar. The spar has a thickness of 3.5 mm and the skin a thickness of 1.6 mm. We modeled five ribs. The skin material is Al2024-T3, the spar material is Al7075-T6. The backside of the WLE is clamped in all degrees of freedom. Contacts are modelled with a Type7 global contact model.

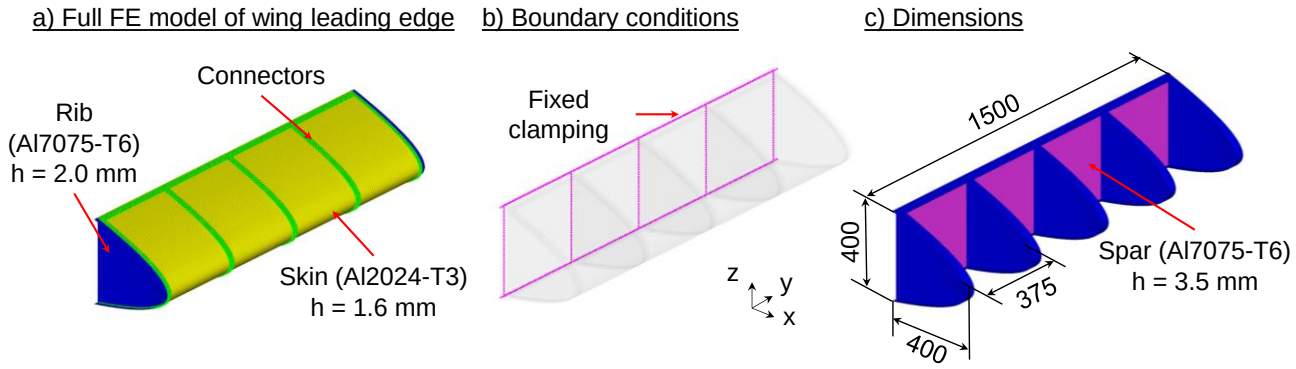

Figure 6: WLE model (see [4])

3.2 Material models

We use the Johnson-Cook (JC) model with damage initiation for Al2024-T3, AlMg3 and the AISI 1006 steel (Table 1 and Table 2). Al7075-T6, M530-50A, Polycarbonate as well as Polyurethane are modeled with an elastic-plastic piecewise linear material model (Table 3). The lithium-polymer cells are modelled according to Sahraei et al. [37] as a stacked pouch model [4]. G-10 glass fiber is used to model the printed circuit boards with data from [6].

Table 1: Johnson-Cook material model parameter (see [4])

	Density ρ [kg/m³]	Young's modulus E [MPa]	Poisson's ratio ν [-]	a [MPa]	b [MPa]	n [-]	c [-]	m [-]	$\dot{\varepsilon}_0$ [-]
Al2024-T3	2770	73000	0.33	369	684	0.73	0.0083	1.7	1
AlMg3	2700	68000	0.3	28.13	278.67	0.183	0.00439	2.527	0.1
AISI 1006	7872	190000	0.3	350	275	0.36	0.022	1.0	1

Table 2: Johnson-Cook damage model parameter (see [4])

	$D1$	$D2$	$D3$	$D4$	$D5$
Al2024-T3	0.112	0.123	-1.5	0.007	0
AlMg3	-0.2	1.133	-0.229	0.0897	7.978
AISI 1006	-0.8	2.1	-0.5	0.002	0.61

Table 3: Elastic-plastic piecewise linear material model parameters

	Density ρ [kg/m³]	Young's modulus E [MPa]	Poisson's ratio ν [-]	σ_y [MPa]	σ_{UTS} [MPa]	$\varepsilon_{\mathrm{UTS}}$ [-]
Al7075-T6	2796	71016	0.33	476	538	0.09
M530-50A	7700	210000	0.3	295	430	0.89
PC	1200	2350	0.3	62	62	0.2
Polyurethane (Foam)	1000	200	0.1	5	5	0.1

4 Results

4.1 Drone Impacts with a Rigid Structure

The contact force-time results for a soft impact on a rigid wall with a flight orientation of 0° are shown in Figure 7 for four impact velocities. We use the coefficient of determination (R^2) to compare the DSM results with the FEA data and the deviation between the load maxima. A good agreement for 80, 100 and 150 m/s impact velocity can be seen. The R^2-score increases from -2.54 up to 0.91 with increasing impact velocity, what indicates a good agreement between FEA and DSM. Local load peaks due to impacts of the various components are reproduced. The slowest speed has large deflections and no agreement between the curves. In case of the highest velocity, the load maxima deviate 7.4 %.

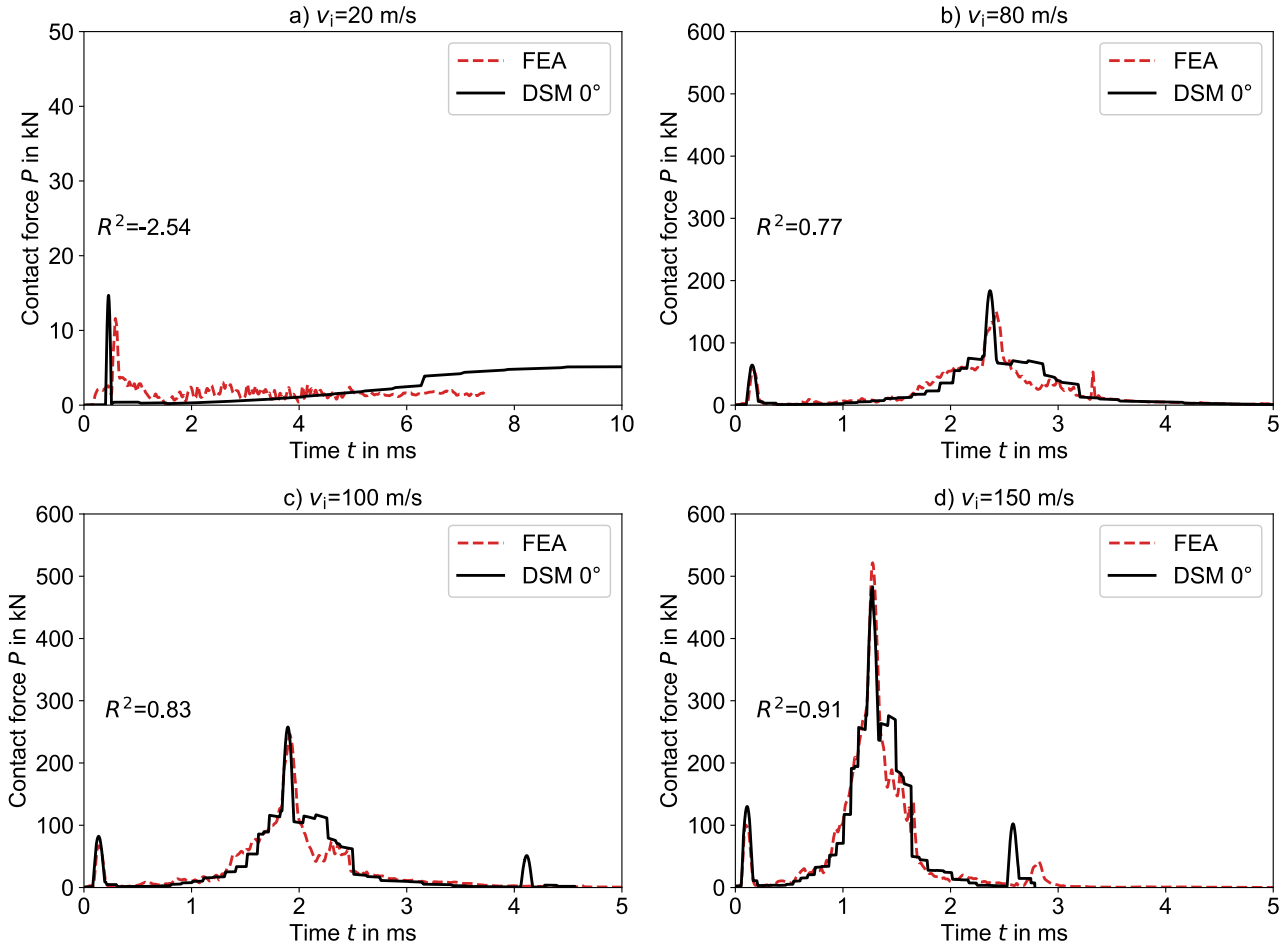

Figure 7: Soft impact on a rigid wall with a flight orientation of 0°

The results for a 45° flight orientation are generally similar (see Figure 8). The slowest velocity shows large deviations regarding the load maximum and the coefficient of determination. We expect that there is a lower limiting velocity that restricts the range of validity of the model. For increasing velocities there is a good agreement of the curves. The R^2-score increases from 0.50 for 80 m/s to 0.57 for 150 m/s. What is interesting in this figure is the qualitative agreement of the curves. Quantitatively, there are still deviations, especially in the load peaks. Several factors may play a role in influencing these deviations. The substitute stiffness seems to be dependent from the impact velocity. Furthermore, the simplification to a 1-D line model neglects inertia effects. Finally, the DSM has velocity limits, which will be discussed in chapter 4.4.

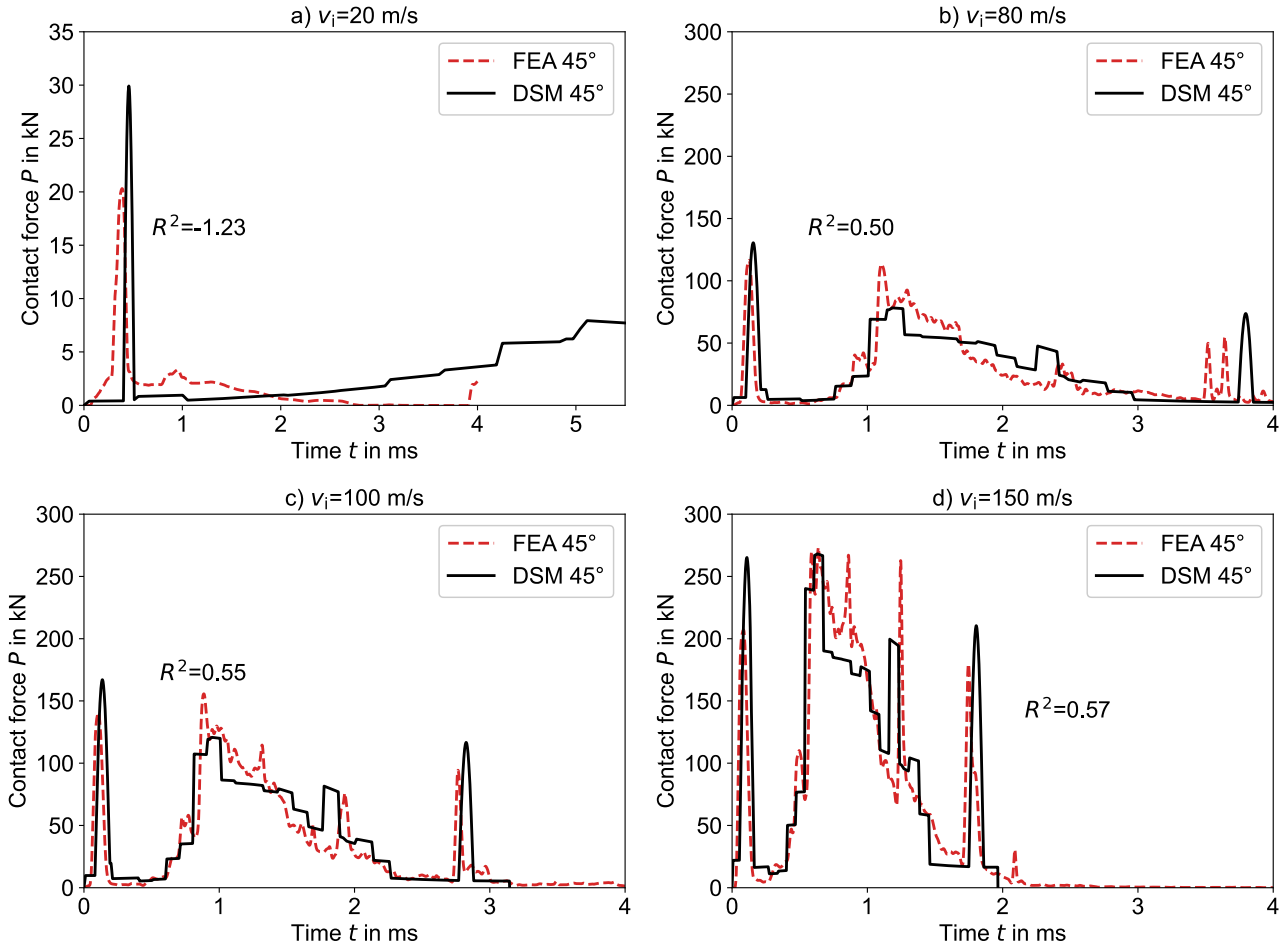

Figure 8: Soft impact on a rigid wall with a flight orientation of 45°

4.2 Drone Impacts with a Deformable Structure

The target structures investigated within this chapter may deform during the impact process. Furthermore, damage can occur. This makes the assumption valid, that all impacts can be declared as hard impacts. That means, that target and projectile behavior are coupled. The projectile may perforate the target, what indicates the need for an upper velocity limit of the model. The model is not developed to describe degradation of the structure due to damage.

As expected from the results for soft impacts, the DSM calculation of the slowest velocity develops large deviations compared to the simulation data for both the 0° (Figure 9) and the 45° (Figure 10) flight orientation. The R^2-score is -2.57 in case of the 0° orientation and 0.04 in case of a 45° orientation. The 0° orientation shows an increase in agreement between DSM and FEA for 80 and 100 m/s. Deviations occur in the area around the load maximum, especially for the 45° orientation. This load maximum is induced due to the impact of the drone center with its battery. The battery is the component of the drone with the largest mass. Due to the explosion risk, the battery model has not yet been validated with dynamic impact test data, which explain these deviations. Furthermore, the neglection of mass summation at the interface may lead to an underestimation of the impact load peaks. The DSM assumes that the undamaged part of the projectile is rigid. But in reality, there is a summation of internal drone components during the impact process. These components hit the target together, what leads to larger impact forces. This underestimation of the impact force can lead to an undersized structure. The model should not be used at this point without further validation through testing and simulations.

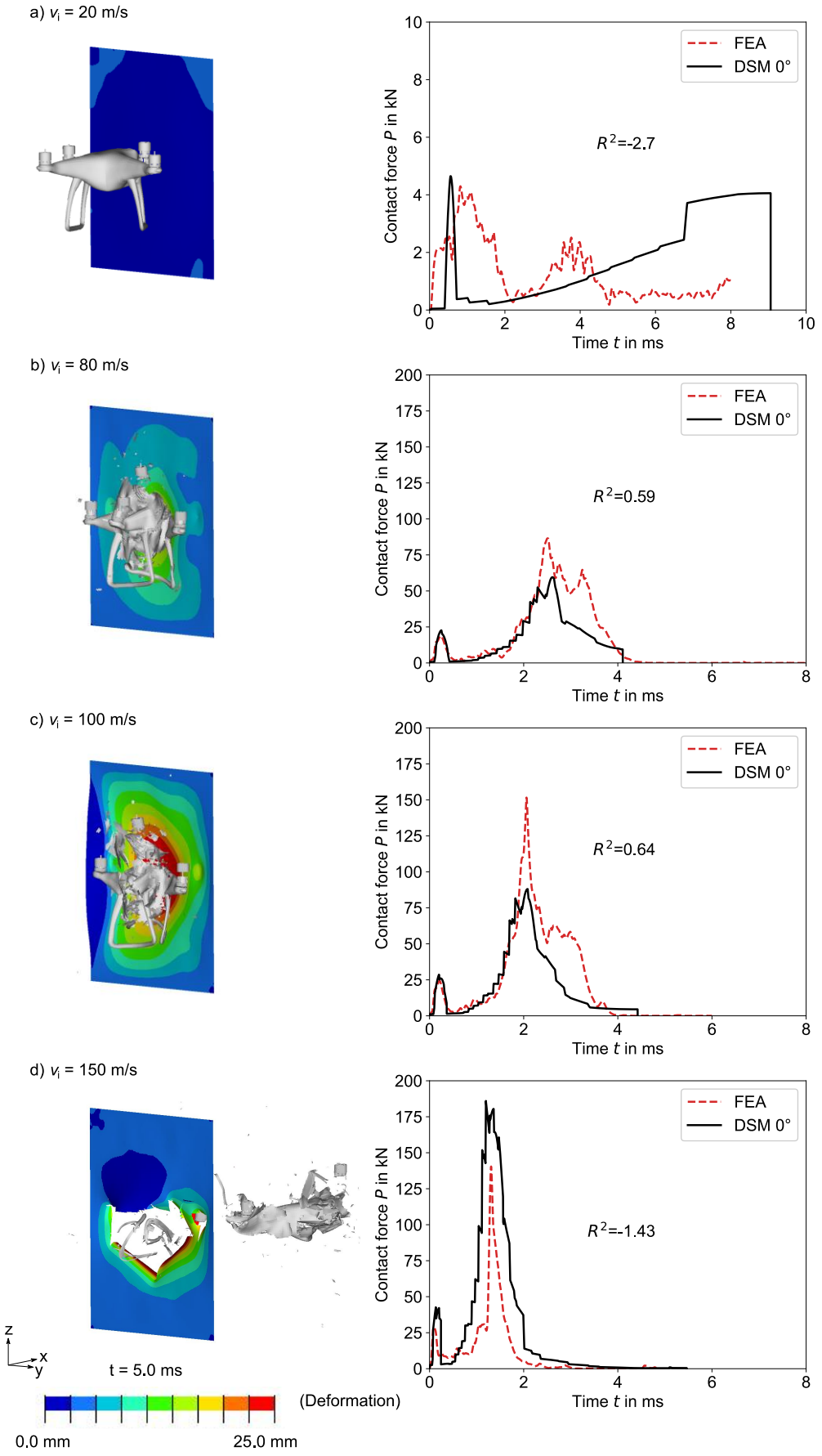

Figure 9: Hard impacts on an Al2024-T3 structure with a flight orientation of 0°

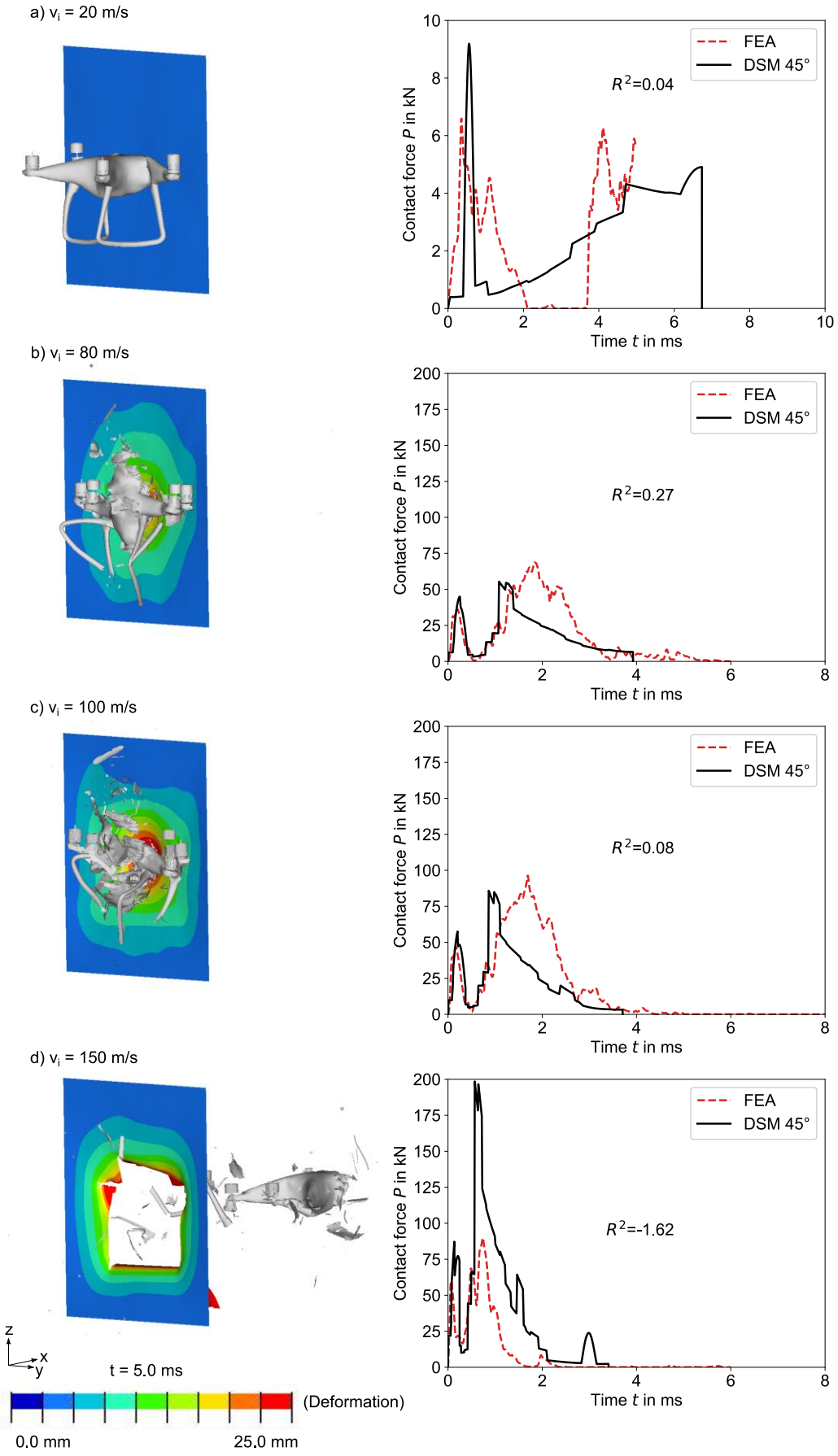

Figure 10: Hard impacts on an Al2024-T3 structure with a flight orientation of 45°

The curves do not agree if the impact velocity is 150 m/s. In this case, the drone perforates the target. This perforation leads to a stiffness degradation of the target, what is not included in the DSM. This degradation produces a smaller impact force of the FEA curve, what can be seen for both flight orientations.

4.3 Drone Impacts with a Wing Leading Edge

In this chapter, we investigate the application of the DSM on realistic drone strikes. The target is a generic wing leading edge. It has a large mass (17.64 kg) compared to the drone projectile (1.38 kg). We assume that the target stiffness k_{t} equals the substitute stiffness k_{e}. If the drone hits the rib of a WLE, the spring stiffness is 3480.5 kN/m. In case of an impact between two ribs the substitute stiffness equals 237.1 kN/m.

The central impact on a rib is shown in Figure 11 for both flight orientations and four impact velocities. If the projectile has an initial velocity of 150 m/s it perforates the target structure, regardless of the flight orientation. Fragments of the drone may hit the wing box, which can cause catastrophic or fatal accidents. The drone projectile does not perforate the WLE for slower velocities. Nevertheless, severe plastic deformations and cracks in the skin occur. The drone itself shatters for velocities higher than 80 m/s. If the impact velocity equals 20 m/s, the drone is deflected along the skin of the WLE and the arms of the drone break. The force curves of the DSM and FEA for this velocity show no agreement, which was to be expected based on the previous results as the lower limit velocity is not reached. A qualitatively agreement can be seen for higher velocities. The load maxima of the curves occur at the same times, but show large differences in the values. The difference is 30 kN for 100 m/s and 135 kN for 150 m/s due to the damage of the WLE. As the DSM results are conservative, this model can be used for preliminary investigations but no detailed structural design.

The results for drone impacts between two ribs are illustrated in Figure 12. Compared to the impacts on a rib, greater damage occurs. Above 80 m/s, the skin of the WLE tears. If the impact velocity equals 150 m/s, the skin rips completely and the drone may perforate the spar, regardless of the flight orientation. Severe damage develops for an impact velocity of 100 m/s. Minor damage develops in the target if the velocity is 20 m/s but the drone is destroyed.

The force-time curves show similar results as already the impact on the rib. The lowest velocity does not yield comparable curves. For higher speeds, the curves between DSM and FEA are qualitatively similar, but show large deviations in the absolute values. For 80 m/s, in contrast to the previous investigation, there are greater deviations for the 45° orientation. In the curves (e.g. for 150 m/s and 45°) differences of up to 200 kN occur. The large deviations in these cases can be attributed to penetration and perforation of the WLE. This also confirms at application level that if the target structure is damaged, the DSM fails and the deviations become too large.

4.4 Discussion

The application of the DSM on different targets shows that it is not valid for every velocity. It produces good results in case of a rigid target with high velocities. Large deviations occur in all studies for the slowest velocity. Furthermore, if the drone projectile perforates the target, the DSM and the FEA results do not agree. Based on these results, we define a valid velocity range for the DSM. The upper velocity limit equals the ballistic limit velocity v_{50}. If the projectile hits the target with this velocity it will perforate the target in 50 % of all cases. This velocity can be determined with various approaches, e.g. the FAA penetration equation [38].

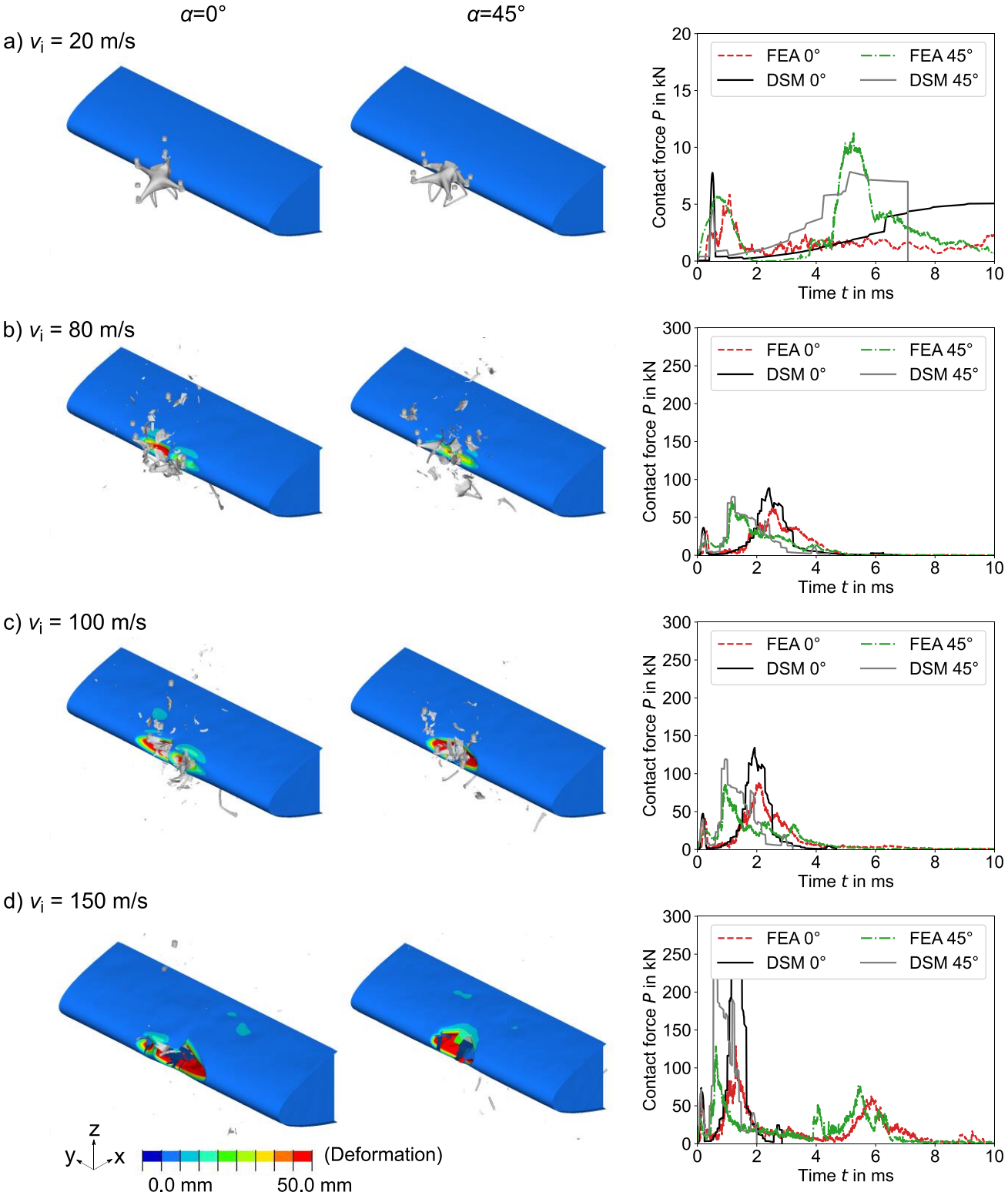

Figure 11: Drone impact on a wing leading edge (rib)

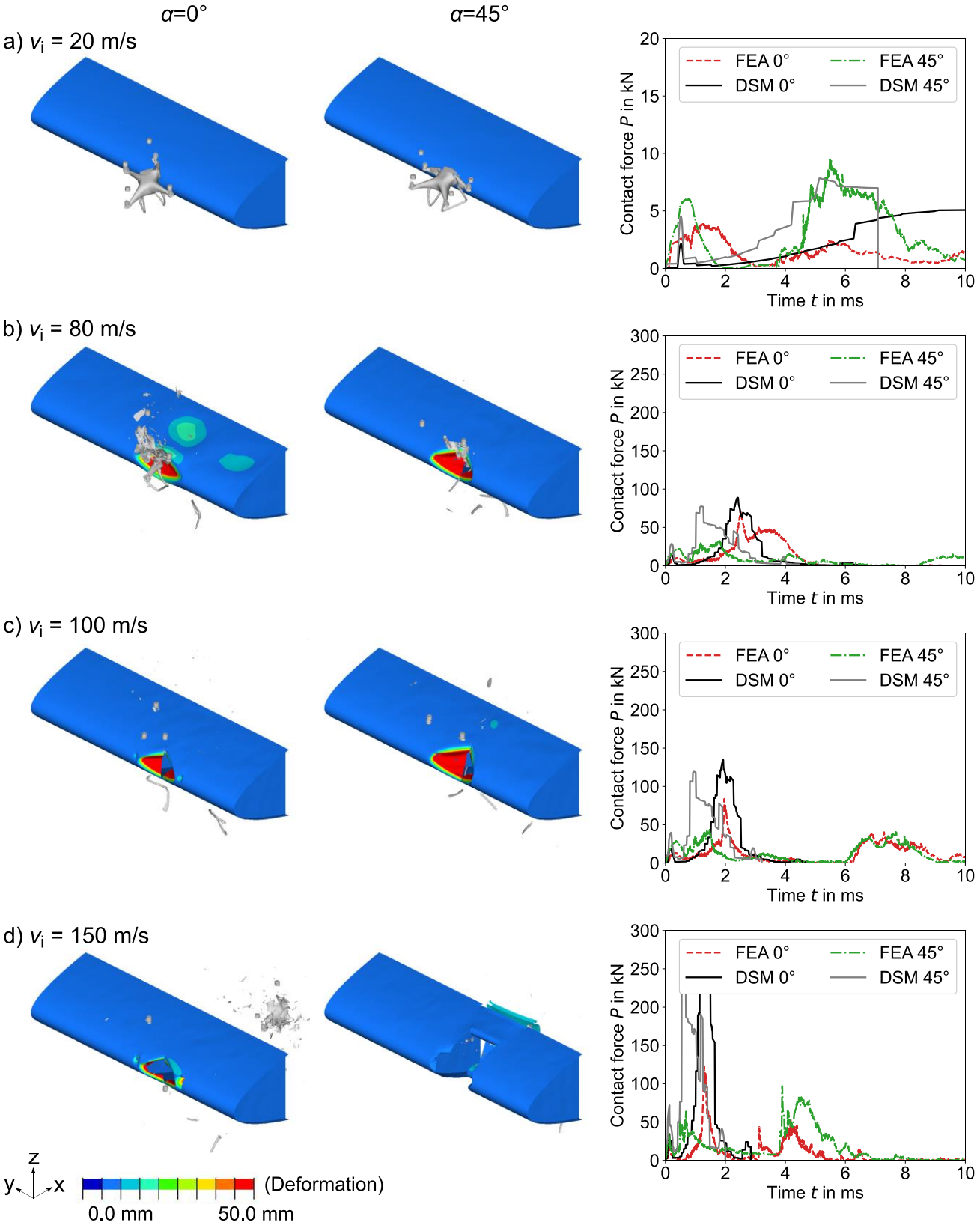

Figure 12: Drone impact on a wing leading edge (skin)

We assume that the energy needed to shatter the projectile determines the lower limit velocity. This energy E_g is the integral of the burst load along the length of the projectile (equation (7)):

$$E_g = \int_0^l P_c(x)\mathrm{d}x \tag{7}$$

Using the conservation of energy, this energy is set equal to the kinetic energy. The lower limit velocity v_{ls} can be determined with the following equation (8):

$$v_{ls} = \sqrt{\frac{2E_g}{m_{pf}}} \tag{8}$$

Further methods like impact tests and FEA can also be used to determine the impact force. All of them have their validity range, as it is shown in Figure 13. The validity range of the DSM is limited and depends on the behavior of the target structure. If the target is deformable, the DSM can be applied for velocities between the lower limit speed and the ballistic limit speed. For rigid targets, there is no ballistic limit, what makes the DSM valid for higher velocities than the v_{50}. Tests and FEA offer the opportunity to investigate lower velocities than v_{ls}. It depends on the impact test setup, but there is a maximum test velocity. FEA does not have this limitation, but models tend to become instable at higher velocities.

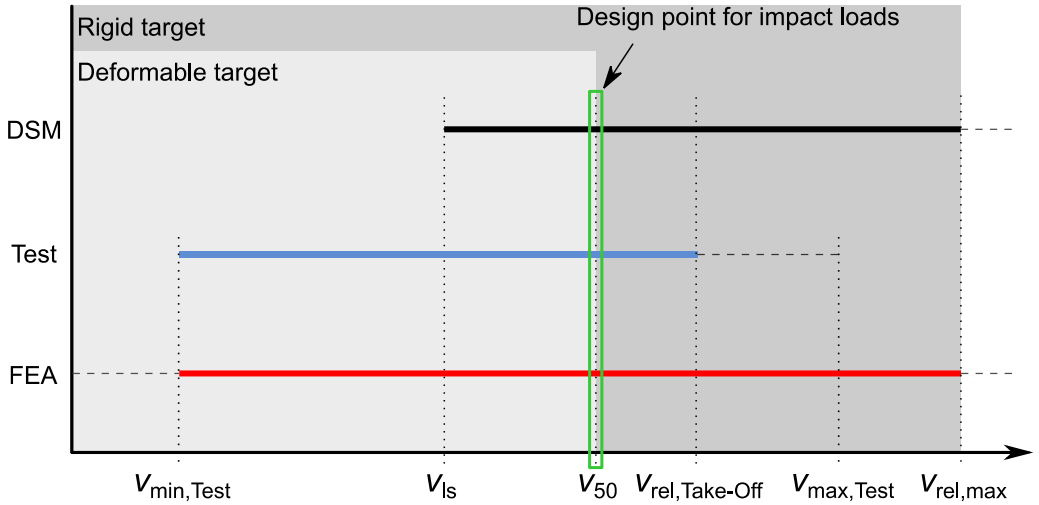

Figure 13: Validity range DSM

The DSM allows a rapid and inexpensive load estimation in the framework of a preliminary design. The impact is a highly nonlinear process. The 1-D spring-mass model and the AIM are vast simplifications and model the impact with a reduced order. Changes in design, material and impact conditions can be investigated in a fast manner with the DSM. If the target is rigid the DSM provides comparable results to FE data. Results from the DSM should not be used for detailed design studies since in application cases it shows large deviations to the FEA results. The DSM can be expanded with a degradation model for the target stiffness to investigate even damaged structures.

5 Conclusion

This paper presents and applies an analytic model to determine the impact force due to drone strikes with various target structures. Current research analyses drone impacts with aircraft structures with tests and finite element simulations. An analytic method gives the engineer the opportunity to analyze drone impacts in a fast and inexpensive manner. The developed drone strike model (DSM) can determine the occurring forces due to an impact of a drone with various target structures. It is developed for impacts with rigid and deformable targets. The DSM is a superposition of the aircraft impact model and a spring-mass model for impacts. Within this paper it is applied on three levels: drone strikes with rigid targets, drone strikes with generic deformable targets and drone strikes with wing leading edges. The DSM results are compared with FEA data from these investigation levels. The DSM produces good results in case of high impact velocities and rigid targets. If the target is deformable, larger deviations occur but the results are qualitatively comparable. The DSM is not able to model damage and the related degradation of the target stiffness. It is valid between the lower limit velocity and the ballistic limit of the target structure. The DSM enables the engineer to perform a rapid and inexpensive load estimation in the framework of a preliminary design. It can be used to investigate the influence of design, material or flight parameter changes on the impact force. It cannot be used for detailed structural design without further development and validation through testing.

6 Contact Author Email Address

Contact: uli.burger@thi.de; florian.franke@thi.de

7 Acknowledgement

This research work is financed by the German Federal Ministry of Education and Research within the funding program "Forschung an Fachhochschulen" under the contract sign DESIRE – 13FH581IX6.

8 Copyright Statement

9 References

[1] UK Airprox Board. Drones UK Airprox Board. https://www.airproxboard.org.uk/Topical-issues-and-themes/Drones/, 2021.
[2] German Air Traffic Control. Sicherheit in der Luftfahrt. https://de.statista.com/statistik/daten/studie/655281/umfrage/behinderungen-des-luftverkehrs-durch-zivile-drohnen-in-deutschland/, 2021.
[3] Franke F, Burger U and Hühne C. Models and Methods for Drone Strike Load Predictions. *Proceedings of the 32nd Congress of the International Council of the Aeronautical Sciences.* Shanghai, 2021.
[4] Franke F, Slowik T, Burger U and Hühne C. Numerical Investigation of Drone Strikes with Various Aircraft Targets. *AIAA SCITECH 2022 Forum,* San Diego, CA & Virtual, 2022.
[5] Franke F, Schwab M, Burger U and Hühne C. An analytical model to determine the impact force of drone strikes. *CEAS Aeronaut J*, Vol. 13, pp 69–84, 2022.
[6] Gerardo O, Gomez L, Espinosa J, Baldridge R, Zinzuwadia C and Aldag T. Volume II - UAS Airborne Collision Severity Evaluation. Springfield, FAA, 2, July 2017.
[7] Gettinger D and Michel A. Drone Sightings and Close Encounters: An Analysis,

https://dronecenter.bard.edu/files/2015/12/12-11-Drone-Sightings-and-Close-Encounters.pdf, 2015.
[8] Song Y, Schroeder K, Horton B and Bayandor J. Advanced Propulsion Collision Damage due to Unmanned Aerial System Ingestion. *30th Congress of the International Council of the Aeronautical Sciences,* Seoul, 2016.
[9] Song Y, Horton B and Bayandor J. Investigation of UAS Ingestion into High-Bypass Engines, Part 1. *58th AIAA/ASCE/AHS/ASC Structures, Structural Dynamics, and Materials Conference,* American Institute of Aeronautics and Astronautics, 2017.
[10] Schroeder K, Song Y, Horton B and Bayandor J. Investigation of UAS Ingestion into High-Bypass Engines, Part 2. *58th AIAA/ASCE/AHS/ASC Structures, Structural Dynamics, and Materials Conference,* American Institute of Aeronautics and Astronautics, 2017.
[11] Bayandor J, Song Y and Schroeder K, *Crashworthiness for Aerospace Structures and Hybrids (CRASH) Lab Virginia Tech*, 01.10.2016.
[12] Lyons T and D'Souza K. Parametric Study of a [sic] Unmanned Aerial Vehicle Ingestion Into a Business Jet Size Fan Assembly Model. *J. Eng. Gas Turbines Power*, Vol. 141, pp 71002, 2019.
[13] Liu H, Man M and Low K. UAV airborne collision to manned aircraft engine: Damage of fan blades and resultant thrust loss. *Aerospace Science and Technology*, Vol. 113, pp 106645, 2021.
[14] Che Man M, Liu H, Ng B and Huat Low K. Preliminary Evaluation of Thrust Loss in Commercial Aircraft Engine due to Airborne Collision with Unmanned Aerial Vehicles (UAVs). *2020 International Conference on Unmanned Aircraft Systems (ICUAS),* Athens, Greece, pp. 1425–1432, 01.09.2020 - 04.09.2020.
[15] Che Man M, Liu H and Low K. Severity assessment of aircraft engine fan blades under airborne collision of unmanned aerial vehicles comparable to bird strike certification standards. *Proceedings of the Institution of Mechanical Engineers, Part G: Journal of Aerospace Engineering, pp* 095441002110449, 2021.
[16] Liu H, Hasrizam Che Man M, Ng B and Low K. Airborne collision severity study on engine ingestion caused by harmless-categorized drones. *AIAA Scitech 2021 Forum,* VIRTUAL EVENT, 2021.
[17] Liu H, Mohd H, Ng B and Low K. Airborne Collision Evaluation between Drone and Aircraft Engine: Effects of Position and Posture on Damage of Fan Blades. *AIAA AVIATION 2020 FORUM,* p. 26, 2020.
[18] Hou N. Dynamic Response and Damage of the Fan Blades during UAV Ingestion into an Aero-Engine. *Proceedings of the 32nd Congress of the International Council of the Aeronautical Sciences,* Shanghai, 2021.
[19] Yu J, LI B, Liu J, Hou N, Zhang Y, Wang Y and Li Y. Numerical simulation of a UAV impacting engine fan blades. *Chinese Journal of Aeronautics*, Vol. 34, pp 177–190, 2021.
[20] Wang Y-H, Wu Z-J and Yang M. The Damage Prediction and Simulation for the UAV and Birdstrike Impact on Wing. *Computer Simulation, pp* 42-45;83, 2018.
[21] Drumond T, Greco M, Cimini C and Medeiros E. Evaluation of Alternative Materials in a Wing Fixed Leading Edge to Support UAS Impact. *Proceedings of the XL Ibero-Latin-American Congress on Computational Methods in Engineering,* Natal, 2019.
[22] Drumond T, Greco M and Cimini C. Evaluation of Increase Weight in a Wing Fixed Leading Edge Design to Support UAS Impact. *Proceedings of the 10th Aerospace Technology Congress, 2019, Stockholm, Sweden,* pp. 71–80, 2019.
[23] Drumond T, Greco M and Cimini C. Numerical analysis of an UAS impact in a reinforced wing fixed leading edge, *J Braz. Soc. Mech. Sci. Eng.*, Vol. 43, 2021.
[24] Meng X, Sun Y, Yu J, Tang Z, Liu J, Suo T and Li Y. Dynamic response of the horizontal stabilizer during UAS airborne collision. *International Journal of Impact Engineering*, Vol. 126, pp 50–61, 2019.
[25] Lu X, Liu X, Zhang Y, Li Y and Zuo H. Simulation of airborne collision between a drone and an aircraft nose. *Aerospace Science and Technology*, Vol. 118, pp 107078, 2021.
[26] Lu X, Liu X, Li Y, Zhang Y and Zuo H. Simulations of airborne collisions between drones and an aircraft windshield. *Aerospace Science and Technology*, Vol. 98, pp 105713, 2020.
[27] Dadouche A, Greer A, Galeote B, Breithaupt T, Vidal C and Gould R. Drone impact assessment

on aircraft structure: windshield and leading edge testing and analysis. March 2020.
[28] Harker M, Horridge S, Harrison R, McNeil J and Abdulrahim M. Testing Aircraft Structural Damage Sustained Due to Collision Impacts with Racing Drones. *AIAA SCITECH 2022 Forum.* San Diego, CA & Virtual, 2022.
[29] Ritt S, Höfer F, Oswald J and Schlie D. Drone Strike on a Helicopter Canopy Demonstrator. *Proceedings of the 47th European Rotorcraft Forum,* Virtual, 2021.
[30] Jonkheijm L, *Predicting helicopter damage caused by a collision with an Unmanned Aerial System using explicit Finite Element Analysis,* Delft, 21.08.2020.
[31] Jonkheijm L, Chen B and Schuurman M. Predicting Helicopter Damage Caused by a Collision with an Unmanned Aerial System Using Explicit Finite Element Analysis. *AIAA SCITECH 2022 Forum,* San Diego, CA & Virtual, 2022.
[32] Slowik T, *Finite-Element-Analysen von Drohnenschlägen auf Luftfahrzeugbauteile,* Ingolstadt, 24.08.2021.
[33] Cairns S, Wood L and Johnson G. Volume I - UAS Airborne Collision Severity - Projectile and Target Definition. Federal Aviation Administration, 16.12.2016.
[34] Gerardo O, Lacy T, Gomez L, Espinosa J, Baldridge R, Zinzuwadia C, Aldag T, Kota K, Ricks T and Jayakody N. Volume III - UAS Airborne Collision Severity Evaluation. Springfield, FAA, July 2017.
[35] D'Souza K, Lyons T, Lacy T and Kota K. Volume IV - UAS Airborne Collision Severity Evaluation. Springfield, FAA, July 2017.
[36] Laczák L and Károlyi G. On the impact of a rigid–plastic missile into rigid or elastic target. *International Journal of Non-Linear Mechanics*, Vol. 91, pp 1–7, 2017.
[37] Sahraei E, Hill R and Wierzbicki T. Calibration and finite element simulation of pouch lithium-ion batteries for mechanical integrity. *Journal of Power Sources*, Vol. 201, pp 307–321, 2012.
[38] Radi A. Potential damage assessment of a mid-air collision with a small UAV. Civil Aviation Safety Authority, 12.6.2013.